J Mater Sci (2006) 41:5151–5160
DOI 10.1007/s10853-006-0438-4

Grain boundary grooving in molybdenum bicrystals

E. Rabkin · A. Gabelev · L. Klinger · V. N. Semenov · S. I. Bozhko

Received: 20 September 2005 / Accepted: 10 March 2006 / Published online: 18 July 2006

Abstract The morphologies of grain boundary grooves formed after annealing of three Mo bicrystals at the temperature close to the melting point were studied with the aid of scanning force microscopy. The ratio of grain boundary to surface energy was calculated from the surface slopes measured at the root of the groove. This ratio was about 0.3 for the grain boundary grooves with the sharp roots, and it was significantly lower than 0.3 for the grooves with the blunted roots. It was shown that the blunting of the root of the grain boundary grooves is associated with the grain boundary migration during annealing. A model of grain boundary grooving accompanied by the instantaneous boundary shift was formulated. The surface topographies predicted by the model were in a good agreement with the experimentally measured ones. It was shown that grain boundary grooving process can be completely suppressed at the singular surfaces. This, together with the grain boundary migration during annealing results in characteristic groove morphology with the blunted root and leads to a significant underestimation of the grain boundary energy calculated from surface slopes.

E. Rabkin (✉) · A. Gabelev · L. Klinger
Department of Materials Engineering, Technion-Israel Institute of Technology, 32000 Haifa, Israel
e-mail: erabkin@tx.technion.ac.il

V. N. Semenov · S. I. Bozhko
Institute of Solid State Physics, Russian Academy of Sciences, 142432 Chernogolovka, Moscow district, Russia

Introduction

Molybdenum exhibits a unique combination of properties, such as high temperature strength combined with good ductility, high Young modulus and low thermal expansion coefficient, which makes it material of choice in many applications. However, molybdenum and its alloys are often prone to intergranular brittleness at and below room temperature, which limits their usefulness as structural materials. Considerable efforts have been undertaken on improving the adhesion at grain boundaries (GBs) in molybdenum by doping it with impurities, most notably carbon [1], and by proper texture [2] and GB character [3] control. It has been shown that the GB fracture stress in molybdenum directly depends on GB energy and, therefore, the knowledge of GB energies can be helpful in design of Mo alloys with increased low-temperature ductility [4]. From the fundamental point of view, molybdenum has been extensively used as a ''test case'' for developing reliable interatomic potentials for body centered cubic (bcc) transition metals. The proper description of interatomic interactions in the transition metals is complicated by the fact that the bonding there is dominated by d-electrons and exhibits some covalent character. This adds a direction-dependent component to the interatomic forces and makes questionable the applicability of central-force interatomic potentials of the Finnis–Sinclair type [5]. Elsaesser and co-workers calculated the energy of symmetrical $\Sigma 5 < 001 >$ tilt GB in Mo (here Σ is the reciprocal density of the coincident sites in two misoriented lattices) using both first-principle total energy calculations and different semi-empirical interatomic potentials and obtained the values in the range of 1.4–2 J/m^2 for the GB energy at

0 K [5]. In the study of Yesilleten and Arias [6] performed with the aid of model generalized pseudopotential theory interatomic potential, a number of symmetric tilt GBs with the <011> misorientation axis were simulated. The calculated values of GB energy varied from 0.61 J/m^2 for the special Σ3(112) GB to 2.18 J/m^2 for the Σ9(122) GB. The calculations of surface energies in Mo using the full charge density method yielded the values in the range of 3.5–3.8 J/m^2 [7]. Since symmetrical Σ5<001> and Σ9<011>(122) GBs in bcc metals usually exhibit the highest energies characteristic for random large angle GBs, it can be concluded that the relative energy (i.e. the ratio γ_b/γ_s, γ_b and γ_s being the GB and surface energies, respectively) of a random GB in Mo at 0 K should be in the range of 0.4–0.6, which is typical for pure metals. At elevated temperatures the relative GB energy may be even higher since it is generally accepted that the excess entropy of free surfaces is higher than that of GBs. However, the experimental measurements of relative GB energies of a number of symmetrical tilt GBs with <011> misorientation axis in high-purity molybdenum yielded very low values in the range of 0.06–0.08 [4]. This large discrepancy between measured relative GB energies and the results of computer simulations is alarming. If the relative GB energies in Mo are indeed as low as reported in [4], the theoretical models used in all above mentioned computer simulations have to be re-considered.

The described discrepancy between experimental measurements and results of computer simulations motivated us to re-examine the process of thermal GB grooving in Mo bicrystals that was used for measuring of relative GB energies in [4]. While the measurements of the dihedral angles at the root of GB grooves were performed with the aid of interference optical microscope in [4], we used a more accurate scanning force microscopy (SFM) technique for measuring surface topography in the GB groove region.

Experimental

Three Mo bicrystals were grown from the misoriented single crystalline seeds by the electron beam floating zone melting technique. The purity of the original material was at least 99.95 at.%. The discs of 10 mm in diameter and 4 mm in height were cut from the as-grown bicrystalline rods by the spark erosion. One surface of the discs was ground and polished by the standard metallographic methods, followed by the electropolishing in the concentrated solution of sulfuric acid at the room temperature. The electropolishing was carried out under 20 V voltage and 10 A/cm^2 current density approximately for 1 min. The discs were fastened with the aid of Mo wire inside the container machined from Mo single crystal of the same purity as investigated bicrystalline samples. The Mo container of the 22 mm of outer diameter and 30 mm of height was placed on Mo wires of 1 mm in diameter laying horizontally on polycrystalline Mo stand installed in the electron beam floating zone melting apparatus. The container could be observed during the heat treatment through the protective lead glass window. After achieving a vacuum of 10^{-6} Torr the container was heated by the defocused electron beam with the gradually increasing power. At the moment at which the outer surface of the container began melting and changing shape the beam power was decreased by 3–4% and the annealing in the achieved steady state regime was carried out for 90 min. According to the optical pyrometer measurements the temperature during annealing was 2400 ± 30 °C. Afterwards, the power of the electron beam was gradually decreased during a few minutes and after the container achieved a temperature of about 1800 °C the beam was switched off.

The surface topography after annealing was studied with the aid of AutoProbe CP SFM (Veeco, USA) operated in the contact mode. W_2C-coated CSC11/50 Ultrasharp Si tips manufactured by NT-MDT (Russia) with the nominal radius of curvature of 50 nm were used. The SPM images contained 256 × 256 pixels and were taken in the region of the GB grooves, with the scanning direction being approximately perpendicular to the groove. The raw data were analyzed with the SPM-integrated PSI ProScan image processing software in order to correct for instrumental distortions. Crystallographic orientations of individual grains were determined by the electron backscattering diffraction (EBSD) method. The acquisition of EBSD patterns (EBSPs) was performed with the LINK OPAL System (Oxford Instruments, UK) mounted on the high-resolution field emission gun scanning electron microscope (HRSEM) LEO982 Gemini (Zeiss–Leica). The EBSPs were taken under the following conditions: accelerating voltage 20 keV, beam current ~3 nA, working distance 21 mm with the sample holder tilted by 70° to the primary beam. The EBSPs were recorded on a CCD and automatically analyzed by the LINK OPAL software.

Results

Figure 1 presents a panoramic optical microscopy (OM) view of the GB in the Sample II. The GB groove

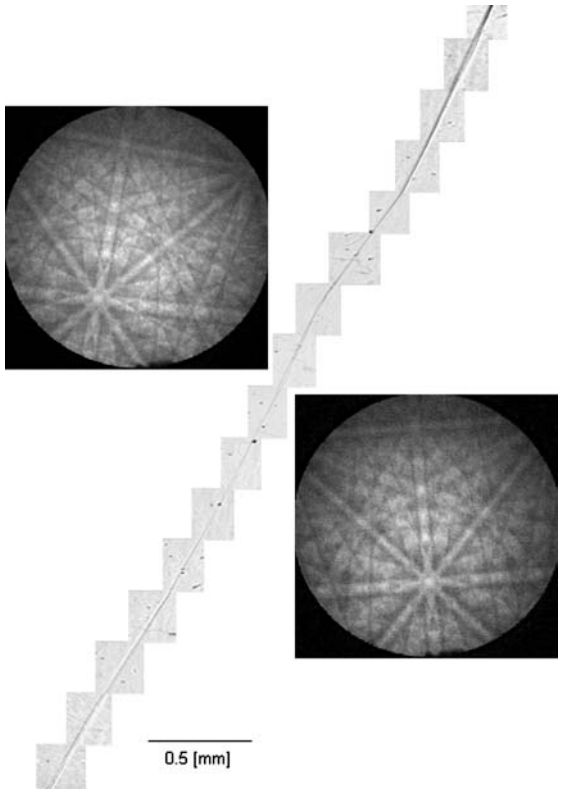

Fig. 1 Panoramic OM view of the GB in Sample II

is clearly visible, and one can see that in the right upper corner of the figure some GB migration occurred that lead to the splitting of the groove. The misorientation parameters of GBs and the plane normals of all grains determined with the aid of EBSD are presented in Table 1. It can be seen that while the GB in Sample I comes close to the special CSL Σ11 GB (50.5° < 011>), according to the Brandon's criterion [8] it is still outside of the angular stability region of this CSL GB. The other two GBs can be classified as random large angle GBs, the GB in Sample II being just at the border between low- and large angle GBs. The misorientation axis of the GBs in Samples I and II are close to < 011> and these GBs are close to the symmetrical tilt ones. The GB in Sample III is close to the twist type, the rotation axis being < 001>.

Figure 2a presents an SFM topography image of a typical GB groove formed in Sample I after annealing. The corresponding topography line profile taken perpendicular to the GB is shown in Fig. 2b. The groove is asymmetric, which is not surprising since two grains forming the GB exhibit different orientations (see Table 1). Moreover, the right-hand side slope of the groove does not exhibit any measurable mathematical curvature, indicating that the anisotropy of surface energy and faceting play a role in the GB grooving process. A surprising feature of the SFM image in Fig. 2a is the blunted root of GB groove. This feature is even more evident on the SFM image (Fig. 2c) and the corresponding line topography profile (Fig. 2d) taken from the same location with higher magnification. Normally, the blunted root of a GB groove indicates that the GB is not there anymore because some GB migration occurred during annealing [9]. In this case the mechanical equilibrium established at the root of the groove while the GB was there gets violated at the moment the GB leaves the groove, and the process of flattening of the abandoned groove begins. The new sharp groove at the final GB position can be observed at some distance from the abandoned groove [9]. However, careful inspection of the bicrystal in the vicinity of the region shown in Fig. 2a did not reveal any new sharp GB grooves. Moreover, the EBSD analyses performed in the groove region indicated that the change of misorientation does occur in the vicinity (±2 μm) of the groove root and, hence, only minor, if any, GB migration occurred during annealing.

Figure 3a demonstrates another typical groove morphology observed at several GB locations in the Sample I. Line topography profile in Fig. 3b clearly demonstrates that within a large GB groove with the blunted root a narrow and sharp new ''sub-groove'' was formed. This is an indication that the GB has moved from the left to the right at the final stages of the annealing, and a new sharp ''sub-groove'' was formed at the final GB position.

In the Sample II, several low angle GBs joining the primary large angle GB were observed. Figure 4 presents a typical OM micrograph of a triple junction between the low angle and large angle GBs. A minor change of the in-plane inclination of the large angle GB at the triple junction indicates that the energy of

Table 1 The geometrical parameters and relative energies of the GBs in the three studies Mo bicrystals.

Sample	I	II	III
GB	56.4 < 6 23 22>	15.4 < 24 −20 3>	43.7 < −1 32 3>
Planes	(53 −42 −5) (−1 1 0)	(61 64 −5) (83 −86 −5)	(−40 −5 34) (7 −22 5)
Deviation From (011), deg	7.8 0.0	3.5 2.6	7.1 30.0
Relative GB energy	0.25 ± 0.01	0.13 ± 0.01	0.32 ± 0.02

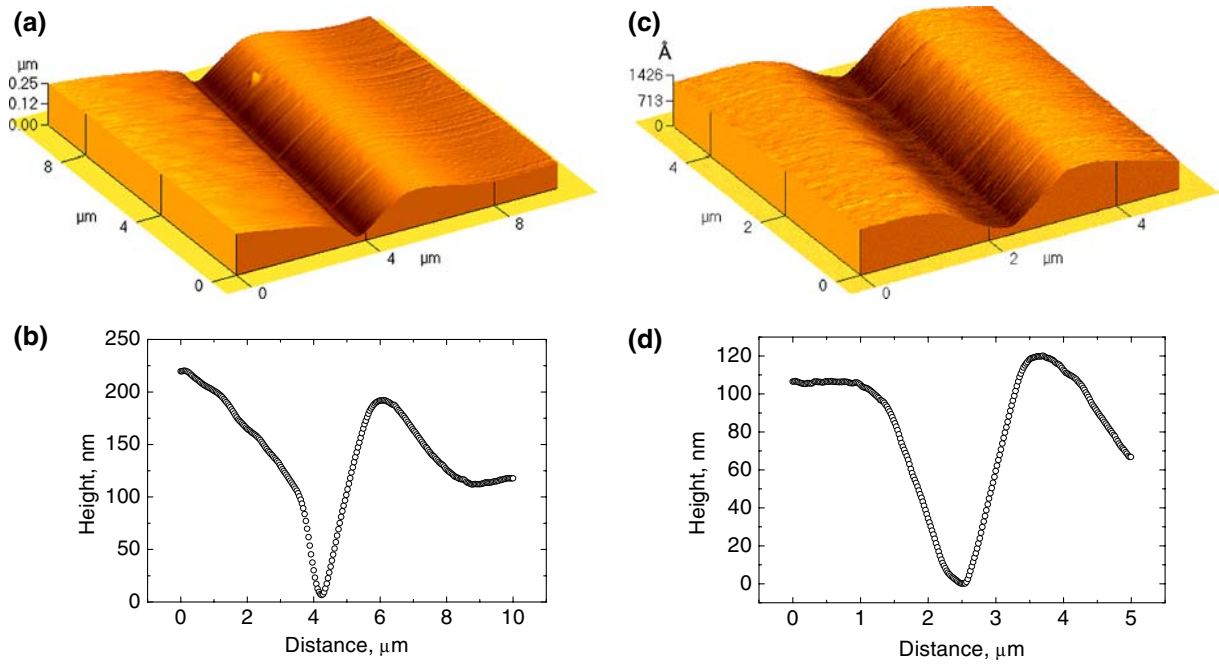

Fig. 2 Typical SFM images of the GB groove region in Sample I (**a**, **c**) and the corresponding topography line profiles (**b**, **d**). The blunted root of the groove is clearly visible in the high magnification images (**c**, **d**)

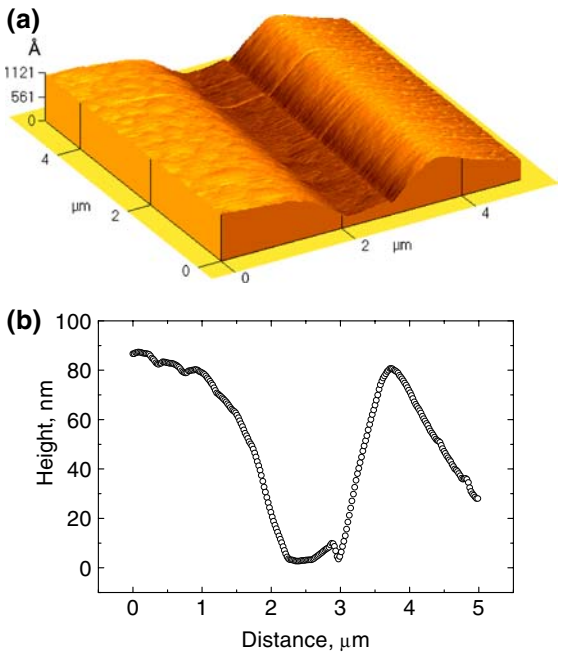

Fig. 3 An SFM image (**a**) and a corresponding line topography profile (**b**) of a channel-like GB groove with the secondary sharp sub-groove observed in Sample I

the low angle GB is very low. The EBSD analyses carried out across the low angle GB did not indicate any change of misorientation, which means that the actual change of misorientation across this GB is below the orientational detection limit of EBSD, which is about 1°.

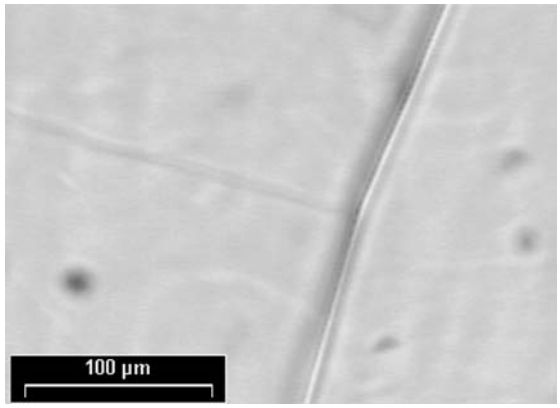

Fig. 4 An OM micrograph of the triple junction of the low-angle and high angle GBs in the sample II

The SFM topography image of the groove formed at the large angle GB in the Sample II in the vicinity of triple junction is shown in Fig. 5a. Also in this case the root of the groove is blunted, which is best illustrated by the line topography profile in Fig. 5b.

Figure 6a presents an SFM topography image of the groove formed at low angle GB in the Sample II in the vicinity of triple junction. The image is noisy because the overall changes in topography are very small and, hence, a very high magnification along the z-axis is used to visualize the GB groove. The corresponding topography line profile in Fig. 6b is too noisy to decide whether the root of GB groove is sharp or blunted.

Figure 7a presents an SFM topography image of a typical GB groove formed in Sample III after

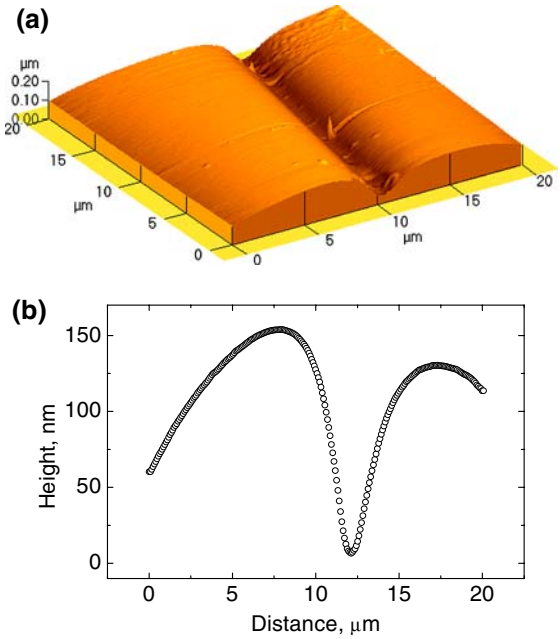

Fig. 5 An SFM image (**a**) and a corresponding line topography profile (**b**) of a typical GB groove in Sample II

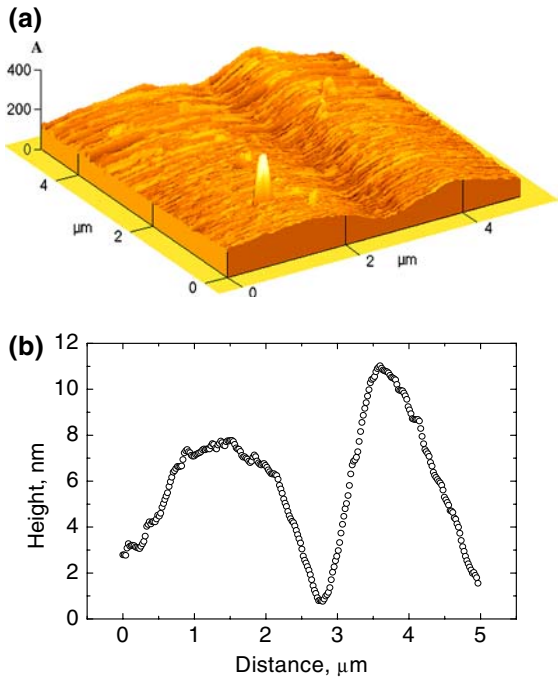

Fig. 6 An SFM image (**a**) and a corresponding line topography profile (**b**) of the GB groove formed by low angle GB in Sample II

annealing. The corresponding topography line profile taken perpendicular to the GB is shown in Fig. 7b. The groove exhibits classical (albeit slightly asymmetrical) Mullins-type morphology [10] with the characteristic sharp root.

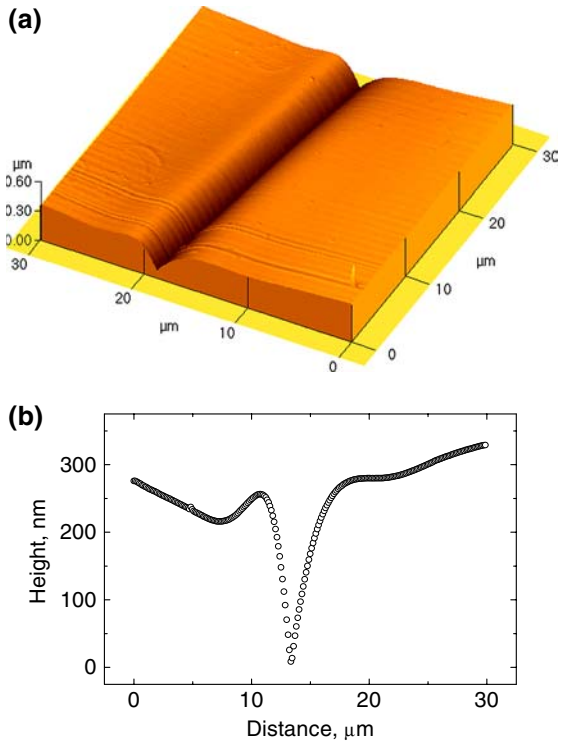

Fig. 7 An SFM image (**a**) and a corresponding line topography profile (**b**) of a typical GB groove in Sample III

Discussion

GB energies

For calculating of the relative GB energy in the case of Sample III we used the procedure developed in the earlier work [11]. Calculating the GB energies in the case of blunted groove roots (Samples I and II) was less straight forward because the exact location of the GB was not known in this case. We estimated the GB energies by the maximal slopes of the two sides of the groove (Fig. 8) according to

$$\frac{\gamma_b}{\gamma_s} = \sin\theta_1 + \sin\theta_2. \quad (1)$$

If the reason for the blunting of the groove root is the GB migration, then the Eq. (1) gives the lower limit of the true value of GB energy. This is because in classical grove morphology the surface slope decreases with increasing the distance from the groove root. Since we extract the slopes at some distance from the location where the GB presumably was located (see Fig. 8), we underestimate the true slopes to the extent proportional to the degree of root blunting. The calculated values of GB energies for all three samples are shown in Table 1. The relative GB energy calculated

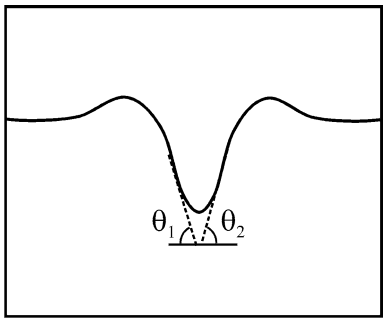

Fig. 8 Schematic illustration of determining the relative GB energy from the topography of GB groove with the blunted root

from the morphology of the sharp sub-groove in Fig. 3 is $\gamma_b/\gamma_s = 0.31 \pm 0.03$. This value is very close to the GB energy in Sample III (exhibiting sharp groove roots). Both values are consistent with the accepted values of the relative GB energies in pure metals [12].

The relative GB energy in Sample II is more than by a factor of two lower than in Samples I and III. We have not found in this sample any sub-grooves or other traces of the GB migration. To a certain extent, it is possible to cross-check the obtained value of GB energy using the geometry of triple junction of the large- and low-angle GBs in this sample (see Fig. 4). The relative GB energy of the low angle GB calculated from the SFM profiles in Fig. 6 is $(\gamma_b/\gamma_s)_{lowangle} = 0.035 \pm 0.006$. This value should be considered as a lower limit for the true relative energy of this GB because the root of the groove is somewhat blunted (though to a lesser extent than the root of large angle GB), and the arguments given above for the large angle GBs in the Samples I and II are also valid for this low angle GB. From Fig. 4, the angles between the large angle GB and the normal to low angle GB are 4 and 5°. A simple condition of mechanical equilibrium at the triple junction neglecting the effects of GB energy anisotropy yields then $(\gamma_b/\gamma_s)_{II} = 0.22 \pm 0.04$ as a lower limit of the relative energy of the large angle GB in the Sample II. This value is closer to the relative GB energies in Samples I and III than the original value (see Table 1) determined from direct measurements of the surface slopes at the blunted GB groove.

From the GB energy measurements reported above we can conclude that whenever the GB groove exhibits a ''classical'', Mullins-type shape with the sharp root the corresponding values of energy are within the usual range of the relative GB energies for pure metals. However, the GB energies formally determined from the topography of the blunted grooves are considerably lower than the GB energies determined from the topography of sharp grooves. It may be that this blunting was overlooked in [4] which led to the underestimation of GB energies.

The surface topography presented in Fig. 3 (Sample I) and exhibiting a blunted primary groove with the adjacent sharp sub-groove provides a strong argument that the observed blunting is associated with GB migration. It is not clear, however, why the topography of the type presented in Fig. 3 was observed just in a few locations in the Sample I, while most of the GB in this sample produced a blunted groove. In the Sample II, no sharp secondary sub-grooves were observed at all, while the EBSD measurements demonstrated that the GB is still located in the groove region. In what follows we will prove that the topography observed in Fig. 3 is indeed associated with GB migration, and that the groove root blunting observed in Samples I and II can be explained by a combination of GB migration and surface energy anisotropy.

GB migration

In [9] it was found that the GBs pinned by thermal grooves in the near-surface region migrate in a jerky, abrupt manner. This inspired us to formulate the following model of coupled GB grooving and GB migration describing the situation of Fig. 3: at the beginning, a symmetrical Mullins-like groove is formed at the initially flat surface (see Fig. 9). The growth of the groove is described by the following governing equation [10]:

$$\frac{\partial y}{\partial t} = -B\frac{\partial}{\partial x}\left(\frac{\partial K/\partial x}{\sqrt{1+(\partial y/\partial x)^2}}\right), \qquad (2)$$

where B is Mullins coefficient

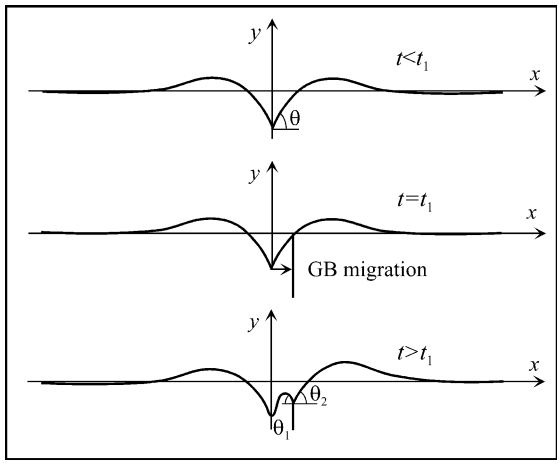

Fig. 9 A model of GB grooving with the instantaneous GB jump during annealing

$$B = \frac{\delta_s D_s \Omega \gamma_s}{kT}, \tag{3}$$

with δ_s, D_s and Ω being the thickness of surface diffusion layer, surface self-diffusion coefficient and atomic volume, respectively. The product kT has its usual meaning, while K is the surface curvature defined by

$$K = -\frac{\partial^2 y/\partial x^2}{\left(1 + (\partial y/\partial x)^2\right)^{3/2}}. \tag{4}$$

The following initial and boundary conditions apply to Eq. (2):

$$\left.\frac{\partial y}{\partial x}\right|_{x=0} = m \equiv \tan\theta; \partial K/\partial x|_{x=0} = 0; y(x \to \infty, t) = 0, \tag{5}$$

where the dihedral angle θ is determined by the mechanical equilibrium at the root of the groove:

$$2\sin\theta = \frac{\gamma_b}{\gamma_s}. \tag{6}$$

The problem defined by Eqs. (2)–(6) is identical to the original Mullins problem [10], except that we allow arbitrary surface slopes. At the moment of time $t_1 < t_0$ (here t_0 is the total annealing time) the GB instantly jumps the distance Δx to the right. For $t > t_1$ the new sub-groove is developing at $x = \Delta x$ in parallel with the blunting of the root at the abandoned GB position. While in the previous work [9] it was assumed that the GB migration distance Δx is much larger than the lateral dimensions of the groove at the original GB position, in this work the situation in which Δx is comparable with the lateral dimensions of the original groove will be considered (see also Fig. 3). To proceed, we need to make some additional assumptions about the GB geometry at the final GB position. We will make the simplest assumption that the GB migrates parallel to itself, and in the final position of the GB its vertical orientation is stabilized by pinning impurities. The same governing Eq. (2) determined the surface evolution also for $t > t_1$, albeit with the different initial and boundary conditions. The ''classical'' Mullins surface topography developed at $t = t_1$ determines the initial condition of the new grooving problem. One boundary condition follows from the condition of mechanical equilibrium at the triple line and is expressed by Eq. (1). Another boundary condition follows from the requirement of the continuity of surface diffusion flux at the root of newly formed sub-groove:

$$\left.\frac{\partial K/\partial x}{\sqrt{1 + (\partial y/\partial x)^2}}\right|_{x=\Delta x-} = \left.\frac{\partial K/\partial x}{\sqrt{1 + (\partial y/\partial x)^2}}\right|_{x=\Delta x+}. \tag{7}$$

We solved the problem formulated above numerically, the details of numerical scheme can be found in [13]. Figure 10 presents an example of the calculated topography profile, compared with the experimentally determined topography from the SFM image in Fig. 3a. In the calculated profile, all lengths are measured in arbitrary units l_0. The units of time are then $\tau = l_0^4/B$. Other parameters employed in calculating the topography profile shown in Fig. 10 are: $m = 0.15$, $t_1 = 5\tau$, $\Delta x = 2l_0$ and $t_0 = 5.5\tau$. An excellent agreement obtained between calculated and experimentally measured profile lends credibility to our hypothesis that the morphology observed in Fig. 3 is associated with the GB migration.

Figure 11 demonstrates the calculated GB groove profile for $t_0 = 9\tau$. A remarkable feature of this profile is its asymmetry, in spite of the fact that in our model we employed isotropic surface energy and surface diffusivity. Formally speaking, for the very long annealing times this profile should evolve to the classical, Mullins-type shape, however, because the surface curvature is relatively low at this stage, such an evolution will be extremely slow. Our model, therefore, provides an alternative explanation to the asymmetry of GB grooves often observed in the experiments [14]: this asymmetry may be a consequence of instantaneous GB

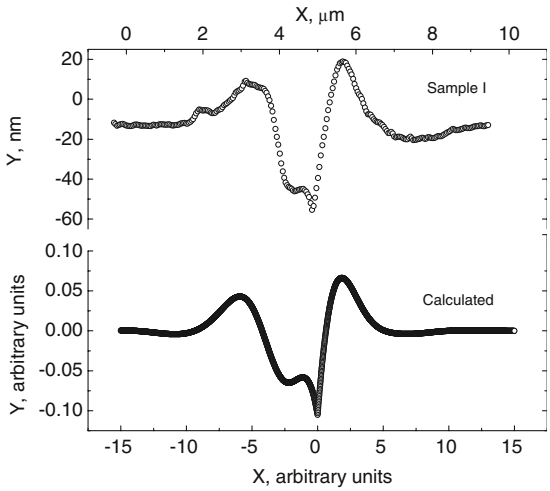

Fig. 10 A comparison of the experimentally measured (Sample I) and calculated line topography profiles

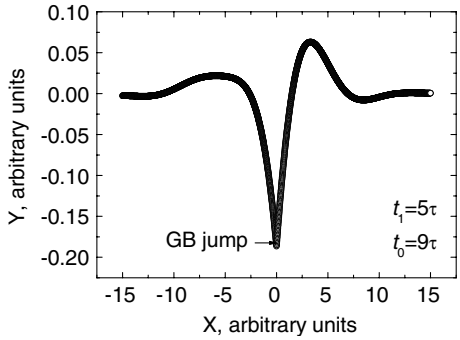

Fig. 11 The calculated GB groove topography profile demonstrating a profound asymmetry

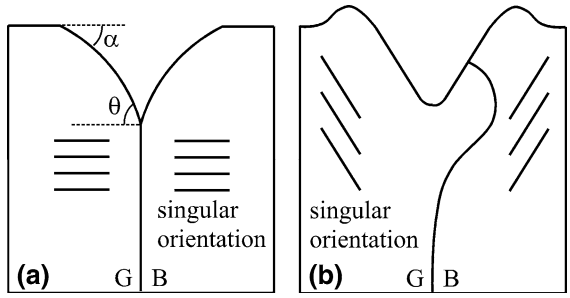

Fig. 12 The GB groove nucleating at the singular surface (**a**) and the morphology produced by migrating GB at the surface slightly deviating from the singular orientation (**b**)

jump during annealing process. It is well possible that the asymmetry of the GB groove profile in Sample III (see Fig. 7) is also associated with the instantaneous GB jump that occurred during annealing, albeit at a much earlier moment of the annealing than in the Sample I. However, both the surface energy and surface diffusivity anisotropy may also contribute strongly to the observed asymmetry.

The role of surface anisotropy

The initial surfaces at which the GB grooving process occurred in the Samples I and II were close to the singular (011) orientations. It is known that in body centered cubic metals this orientation exhibits a local minimum of surface energy [12]. In what follows we will show that this anisotropy may strongly affect the GB grooving process and that a combination of surface anisotropy and slight GB migration explains the blunted groove root morphologies and the absence of any secondary sub-grooves observed in Samples I and II. We will adopt a model of strongly anisotropic surfaces, in which the otherwise spherical surface γ-plot (polar plot of surface energy) exhibits very sharp cusps at singular orientations, the energies of isotropic and singular surfaces being γ_s and γ_0, respectively (obviously, $\gamma_0 < \gamma_s$). Let us first consider the bicrystal with initially singular surfaces at which the GB grooving occurs (Fig. 12a). The condition of mechanical equilibrium at the intersection of the GB with the singular surfaces should include Herring's torque terms, which in the case of very sharp cusp on the γ-plot can be extremely high. This does not mean, however, that the formation of GB groove is impossible in this case. The possibility of GB groove formation should be controlled by the total interfacial energy change, ΔE, associated with the nucleation of a very small groove with the non-singular walls (Fig. 12a). At this nucleation stage the curvature of the non-singular groove walls should be approximately constant (i.e. they should be cylindrical) because the high absolute value of curvature for small grooves: the deviations from high curvature are also high and, because of the small dimensions of the nucleus, the driving force to eliminate those deviations will be high either. If ΔE is negative, then the groove should spontaneously nucleate and grow. A simple geometrical consideration yields

$$\Delta E = -R(\cos\alpha - \cos\theta)\gamma_b - R(\sin\theta - \sin\alpha)\gamma_0 + R(\theta - \alpha)\gamma_s, \tag{8}$$

where R is the radius of curvature of the non-singular wall and the meaning of the angles α and θ is clear from Fig. 12. Here, the contribution of the surface bumps made of the material extracted from the groove region to the total interfacial energy has been neglected. This is justified if the surface diffusion along the singular surfaces is fast so that the material extracted from the groove is distributed over the wide area. The conditions of mechanical equilibrium at the junctions between non-singular wall of the groove and the singular surface, and between the non-singular wall of the groove and the GB are:

$$\gamma_0 = \gamma_s \cos\alpha,\ \gamma_b = 2\gamma_s \sin\theta \tag{9}$$

Combining Eqs. (8) and (9) yields

$$\Delta E = -\gamma_s R\Big[2\sin\theta\Big(\cos\alpha - \cos\theta\Big) + \cos\alpha\Big(\sin\theta - \sin\alpha\Big) + \alpha - \theta\Big], \tag{10}$$

The expression in square brackets of Eq. (10) is positive for

$$\alpha < \theta, \tag{11}$$

which means that for GB grooving to be possible the non-singular walls of the groove should be convex. This

is understandable, since for isotropic surfaces the curvature-related addition to the chemical potential of surface atoms is positive for convex surfaces. For the GB groove to grow, the excess chemical potential at the groove walls should be positive. The threshold value of the relative GB energy, γ_b^*, below which the GB groove will not be formed can be determined by transforming the inequality (11) into equation. Combining Eqs. (9) and (11) gives

$$\frac{\gamma_b^*}{\gamma_s} = 2\sqrt{1 - \left(\frac{\gamma_0}{\gamma_s}\right)^2} \tag{12}$$

For only 3% of surface energy anisotropy ($\gamma_0/\gamma_s = 0.97$), which is not uncommon in metals, we get $\gamma_b^*/\gamma_s \approx 0.49$, i.e. relatively high value of threshold GB energy. All GBs with lower relative energies will not form the grooves at the singular surface of the energy γ_0. In this respect, the GB grooving processes at the anisotropic and isotropic surfaces are very different. While any, even extremely low energy GB should produce a groove at the isotropic surface, surface anisotropy may suppress the GB grooving completely.

From the above consideration of the role of surface anisotropy in GB grooving the following scenario of the GB grooving in Samples I and II emerges: due to minor miscuts and experimental uncertainties the original polished surfaces of the grains were slightly misoriented from exact (011) orientations. At the beginning of heat treatment the anisotropic GB groove with the walls running parallel to (011) planes was formed. The mechanism and growth kinetics of such anisotropic grooves were considered in [15]. It should be noted that a dihedral angle at the root of such anisotropic groove is related to the bicrystal geometry only and has nothing to do with the GB energy. At a certain moment during the treatment the GB migrated slightly and arrived at ideally planar surface with exact (011) orientation (original groove wall) in one of the grains. The GB energy was too low to overcome surface anisotropy at this final GB position, and the new GB sub-groove was not formed at all. At the same time, the process of healing of the sharp root at the abandoned GB position resulted in characteristic blunted root morphology. The SFM observations of the annealed samples revealed the GB grooves with blunted roots and no traces of sharp sub-grooves at the final GB positions. It is possible that a combination of higher GB energy and local variations of surface orientations in the Sample I allowed the barrier for GB grooving at the final GB position to be overcome, which resulted in characteristic morphology of Fig. 3.

Conclusions

From the results of the present study the following conclusions can be drawn:

(1) The GB grooves formed in Mo bicrystals after annealing in the vicinity of the melting point were studied with the aid of SFM. Three typical groove morphologies were observed: (i) Mullins-like, albeit asymmetrical grooves with the sharp root; (ii) grooves with the blunted root, and (iii) grooves with the blunted root with the secondary sub-groove with the sharp root in the region of a primary groove.

(2) The ratio of GB and surface energies determined from surface slopes in the root region for the grooves with the sharp roots was about 0.3, which is a value typical for pure metals. However, significantly lower values were obtained for the grooves with the blunted roots. This may explain the low values of relative GB energy obtained in a previous study [4], since the blunting of the groove root can be easily overlooked in the interference optical micrographs.

(3) It was shown that a characteristic channel-like morphology exhibited by blunted grooves with the secondary sub-groove can be interpreted in terms of instantaneous GB jump during annealing. In this case, the original groove with the blunted root and the secondary groove with the sharp root mark the GB original and final positions, respectively. A model of GB grooving by surface diffusion mechanism taking into account such a jump was formulated. The surface morphologies predicted by the model are in an excellent agreement with the experimentally observed ones.

(4) The EBSD measurements of the crystal orientations demonstrated that the change of orientation occurs in the groove region even for the GB grooves with blunted root that do not exhibit any secondary sub-grooves. To resolve this apparent contradiction (a GB should always produce a sharp groove) we considered the nucleation of the GB groove at the singular surface. It was shown that even a relatively weak anisotropy can suppress the grooving process completely. The blunted groove morphology observed at the tilt <011> GBs was then

explained by a combined effect of surface anisotropy, slight deviations of the grains orientations from the ideal $<011>$, and instantaneous GB jump during annealing.

Acknowledgement This work was supported by the ISTC Project No. 2140 and by the P. and E. Nathan Research Fund.

References

1. Miller MK, Bryhan AJ (2002) Mater Sci Engng A 327:80
2. Huensche I, Oertel CG, Tamm R, Skrotzki W, Knabl W (2004) Mater Sci Forum 467–470:495
3. Watanabe T, Tsurekawa S (1999) Acta Mater 47:4171
4. Tsurekawa S, Tanaka T, Yoshinaga H (1994) Mater Sci Engng A 176:341
5. Ochs T, Elsaesser C, Mrovec M, Vitek V, Belak J, Moriarty JA (2000) Phil Mag A 80:2405
6. Yesilleten D, Arias TA (2001) Phys Rev B 64: (No. 174101)
7. Vitos L, Ruban AL, Skriver HL, Kollar J (1998) Surf Sci 411:186
8. Brandon DG (1966) Acta Met 14:1479
9. Rabkin E, Amouyal Y, Klinger L (2004) Acta Mater 52:4953
10. Mullins WW (1957) J Appl Phys 28:333
11. Amouyal Y, Rabkin E, Mishin Y (2005) Acta Mater 53:3795
12. Martin JW, Doherty RD, Cantor B (1997) Stability of microstructure in metallic systems. Cambridge University Press, Cambridge, UK, p 220
13. Klinger L, Rabkin E (2005) Z Metallkd 96:1119
14. Munoz NE, Gilliss SR, Carter CB (2004) Phil Mag Lett 84:21
15. Klinger L, Rabkin E (2001) Interface Sci 9:55